Early-arrival waveform inversion: Application to cross-well field data

Xukai Shen, Tieyuan Zhu, and Jerry M. Harris

ABSTRACT

We apply early-arrival waveform inversion to a cross-well field data in order to find the extent of a potential reservoir that terminate somewhere between the two wells. Ray-based tomography result is too smooth to resolve the boundary. On the other hand, waveform inversion is able to better utilize the advantage of short wavelength cross-well data, resulting in a velocity model that defines the potential reservoir boundary more sharply. Details from the waveform inversion result are verified by well-log data.

INTRODUCTION

Cross-well data is usually of higher frequency, and therefore shorter wavelength, than surface seismic data. Theoretically, this should enable us to reveal more details of the subsurface structure by performing tomography using cross-well data. However, if ray-based methods (Hampson and Russell, 1984; Olson, 1984; White, 1989) are used, the tomography results do not contain much detail, because ray-based methods are based on the high-frequency approximation, which mandates that the scale of subsurface structures be much larger than the dominant wavelength of the data. Such an approximation results in very smooth velocity models. Waveform inversion (Tarantola, 1984; Pratt et al., 1998; Mora, 1987), on the other hand, does not suffer from such approximation, and is capable of producing a much higher resolution result.

The two wells used to acquire this dataset are located very close together, only 640 feet apart. One well penetrates an anomalous zone, but the other one missed the zone. The anomalous zone contains massive reservoir-quality carbonate, as suggested by the first well. However, surface seismic data in the same area has insufficient resolution to determine the vertical and horizontal extent of the zone. To more accurately identify the boundary of the zone, a cross-well survey was conducted between these two wells.

The cross-well data were collected with a piezoelectric cylindrical bender source and hydrophone receivers in the depth range of 8200-9200 ft (2500-2800 m). A total of 201 source levels were spaced at 5 ft (1.5 m) depth intervals, and 203 receiver levels were also spaced 5 ft apart. This resulted in a raw data set with about 40000 traces. The input signal was a 250-1250 Hz linear upsweep (Langan et al., 1997). Details of the acquisition system and the techniques employed can be found in (Harris et al., 1995). The data retrieved have a relatively good signal-to-noise ratio. The only strong

coherent noise is the tube wave that exists in all shot records (Figure 1), which is caused by potential leakage in the receiver well.

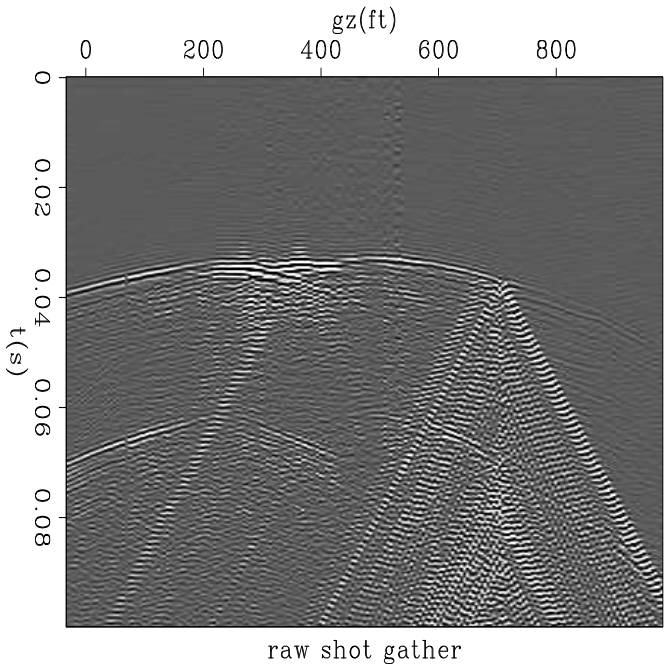

Figure 1: Typical shot gather from the field cross-well dataset. Notice the strong tube wave in the right part of the shot gather. [**NR**]

Previous result from ray-based methods (Langan et al., 1997) is very smooth, and did not identify the boundary of the zone very well. To better define the boundary, we apply early-arrival waveform inversion (Tarantola, 1984; Pratt et al., 1998; Mora, 1987) to the dataset.

INVERSION SETUP

In real-data application of waveform inversion, it is usually more reliable to match kinematics (traveltime) than dynamics (amplitude), since the acoustic wave-equation can not predict field data amplitude very well. The waveform inversion objective function used here is from Shen (2010). Since cross-well data usually contain converted waves, and we want to estimate p-wave velocity only, we choose to match direct arrivals only, which are free of converted energy and can usually be described accurately by the acoustic wave equation. We create a data mask to keep only the direct arrivals in the input data. We also make sure that tube wave is not included in data matching. An example of the data mask applied to a low-passed shot gather is in Figure 2.

Next we need to determine the proper source wavelet for forward modeling during inversion. Direct arrivals at the receiver side acurately represent what the source wavelet looks like. However, we are using two-dimensional modeling, whereas the field data source is a three-dimensional point source. We apply a phase shift to the direct arrival to correct for that. To improve the signal-to-noise ratio of the source

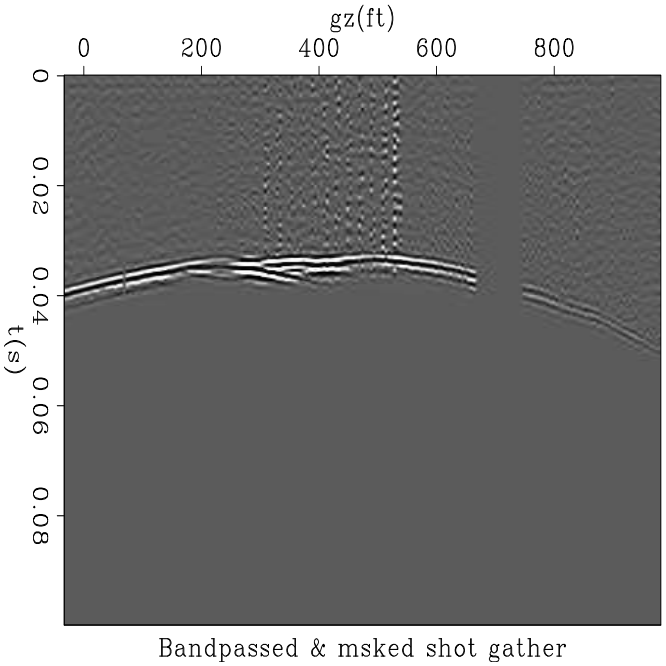

Figure 2: Same shot gather after bandpass and applying data mask. Data mask only keeps direct arrival for inversion purposes. [**NR**]

wavelet, direct arrivals are first aligned by using picked first-break traveltime, then stacked to form the reference source wavelet. In this way, each shot has its own source wavelet. The original source and receiver coordinate has a 1-ft interval increment. However, since our modeling grid has a 5-ft interval in both the x and z directions, the source and receiver coordinates are rounded to a 5-ft grid by nearest-neighbor criteria.

The next element for waveform inversion is the starting model, which we obtain by using ray-based traveltime tomography. The tomography adopts the L2-regularized least-square approach to minimize the difference between observed and calculated traveltimes. We use the finite-difference Eikonal solver to compute the traveltime and then we back-project the raypaths from a receiver to the source (Zelt and Barton, 1998). We solve the objective equation by a Gauss-Newton strategy; for details see (Zhu and Harris, 2011). The observed data are the picked first break times from the full data set. The 2D inverse domain size is 133 by 206 cells, with a total number of 27,398 unknowns. The initial model for traveltime tomography has a constant velocity which is the average velocity value obtained from velocity logs. We ran ten iterations, stopping when the traveltime residuals were no longer significantly decreased. The final root-mean-square (RMS) residuals were reduced to 7.6e-3 ms from the initial value of 1.9 ms. Figure 3 shows the traveltime tomography result.

Comparison of data modeled from initial velocity and input data is shown in Figure 4. The finite difference modeling verified that the initial model predicts the data kinematics quite well in general. Only when traveltime is not continuous does the initial model have trouble producing a good match. Since the initial traveltime tomography result already matches picked first-break traveltime quite well, so the

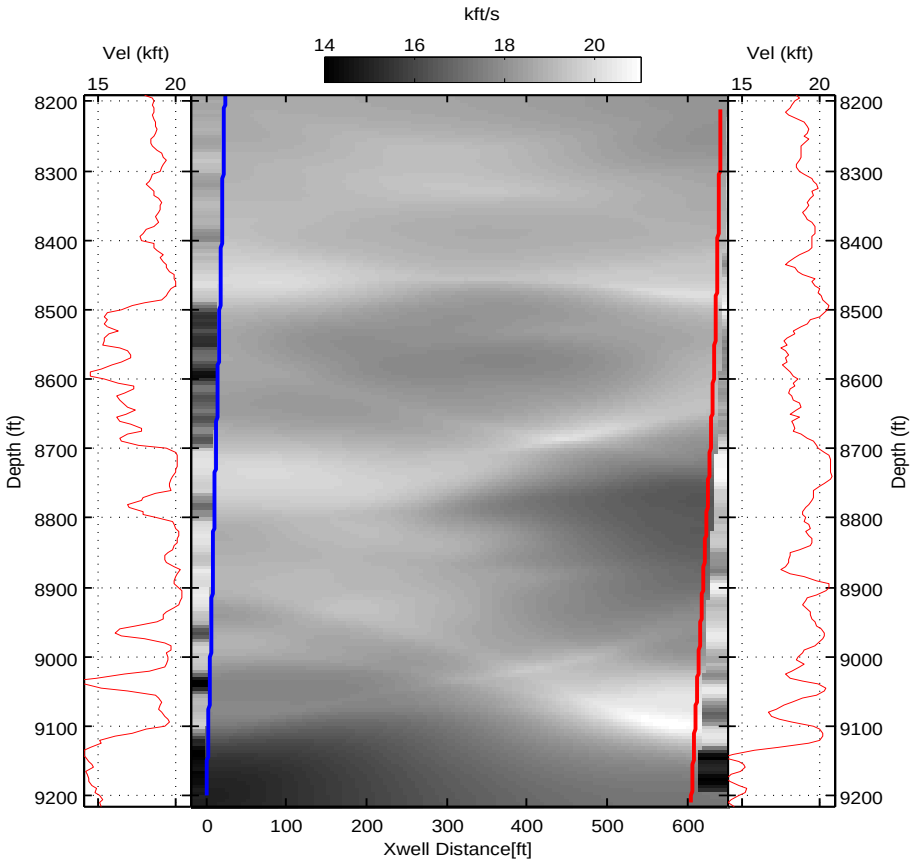

Figure 3: Starting model from traveltime tomography. Left line is receiver well. Right line is source well. Outside wells are well-log velocity values. [**NR**]

waveform inversion result mainly adds details to the traveltime tomography result.

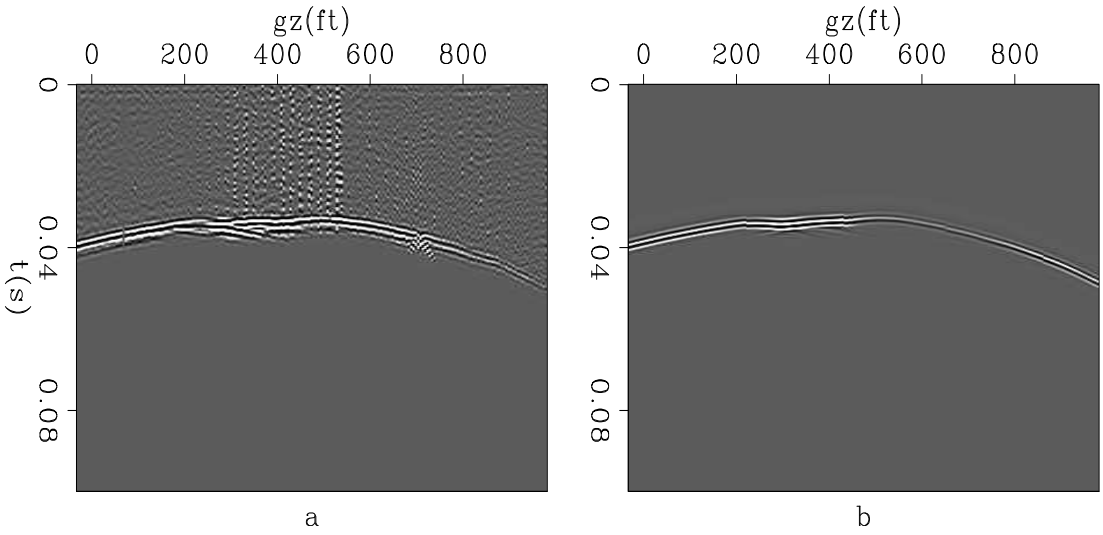

Figure 4: Same shot gather as before, comparsion of input first arrival and data modeled from the tomography result. The two are already very similar in terms of kinematics. a): Input first arrival; b): first arrival modeled from the tomography result. [**NR**]

RESULT ANALYSIS

A total of 180 shots are used. Two passes of inversion are run. First with data bandpassed between 200 Hz and 400 Hz, then with data bandpassed between 200 Hz and 700 Hz. The final inversion result is shown in Figure 5, with well location indicated by the two slanted lines, and the well velocity value outside the red slanted lines. The inversion result matches well-log data reasonably well, and it better defines the extent of the anomaly, which is also consistent with well-log data. Compared to the tomography result, there are more details in the waveform inversion results. There are some thin layers that are present in the well-log and waveform inversion results, yet are missing in the traveltime tomography result.

RMS data residual as a function of iteration numbers is shown in Figure 6. Since the initial model is already quite close to the true model, the RMS data residual did not reduce as drastically as expected. A typical shot-gather residual is shown in Figure 7 and 8. It can be seen that data residuals have been reduced mostly in the center part, where rays do not describe the kinematics well.

Comparing the forward-modeled first arrival from the initial velocity, the forward-modeled first arrival from the final velocity, and the input first arrival (Fig 4 and 9), the major improvement comes from kinematics matching. This is not surprising, given the inversion objective function we use. The first arrival modeled from initial velocity is continuous, even where the input first arrival is not. Such discontinuity is

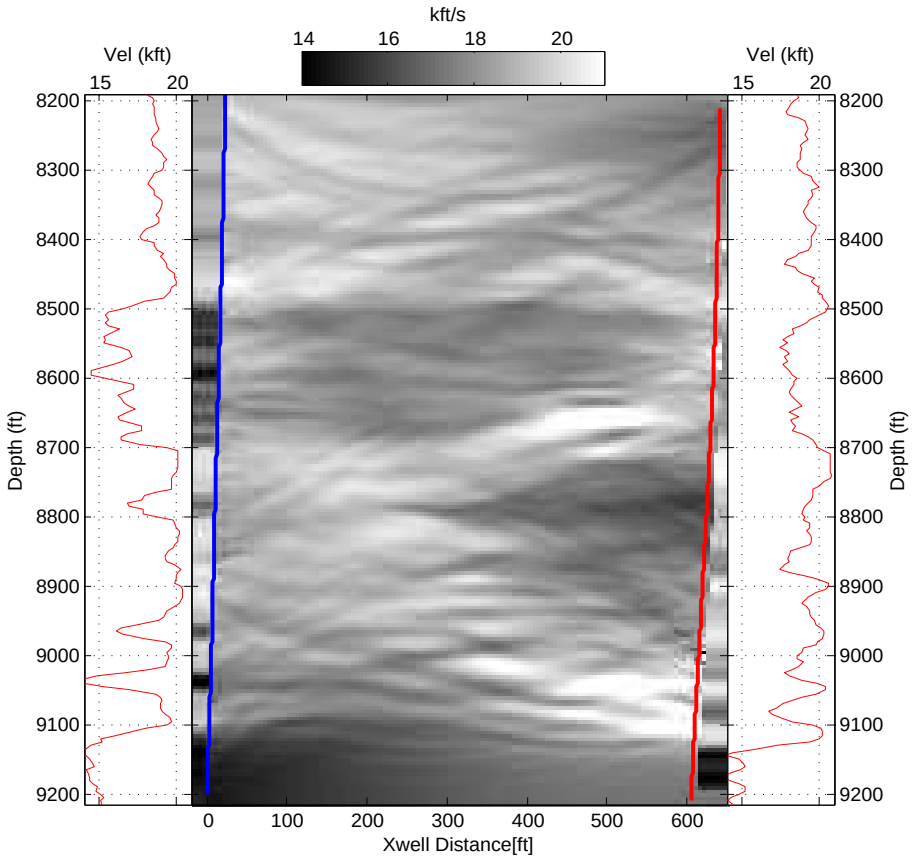

Figure 5: Final model after waveform inversion. Left line is receiver well. Right line is source well. Outside wells are well-log velocity values. [**NR**]

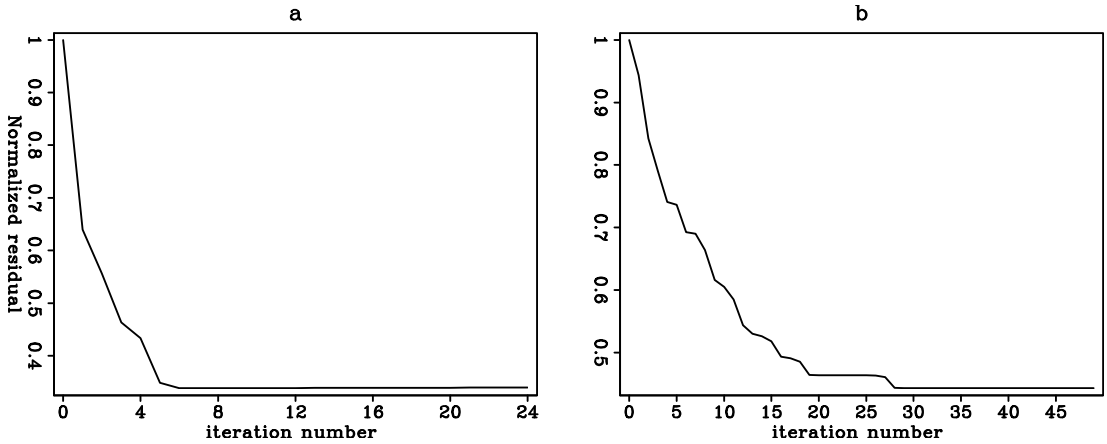

Figure 6: Data residual of the two inversion steps. a): Normalized residual of 200-400 Hz inversion. b): Normalized residual of 200-700Hz inversion. [**NR**]

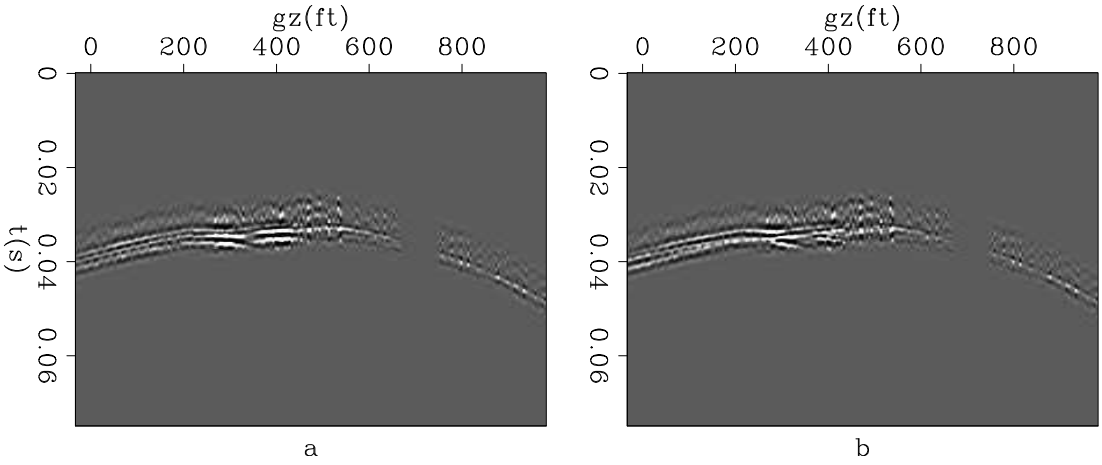

Figure 7: Shot residual of the first inversion steps. a): initial residual. b): final residual. [**NR**]

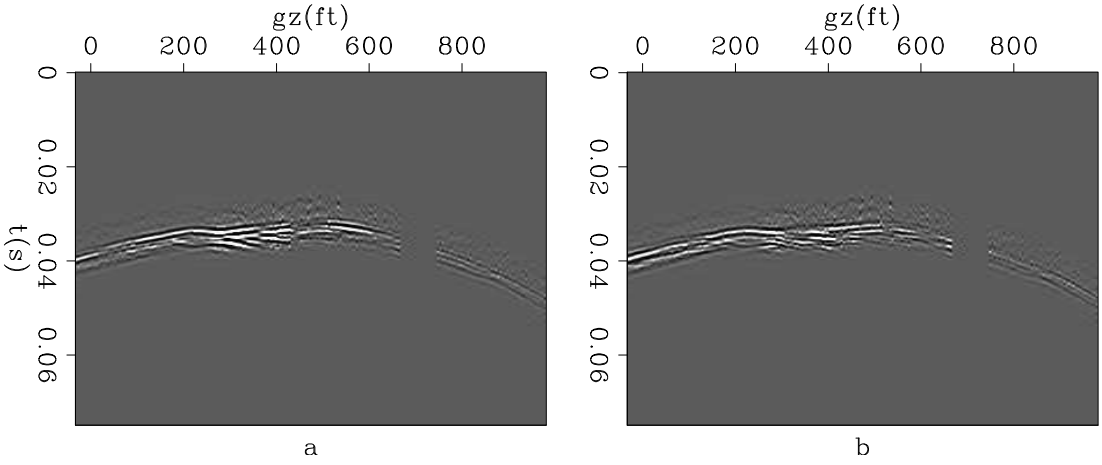

Figure 8: Shot residual of the second inversion steps. a): initial residual. b): final residual. [**NR**]

captured in the first arrival modeled from the final model. Since such discontinuity can be explained better by wave phenomena, ray-based inversion methods can not accurately handle it. Another advantage of waveform inversion is its capability of modeling more than first arrivals. Data modeled from the final velocity predict some later arrivals which do not show up in the data modeled from the initial velocity.

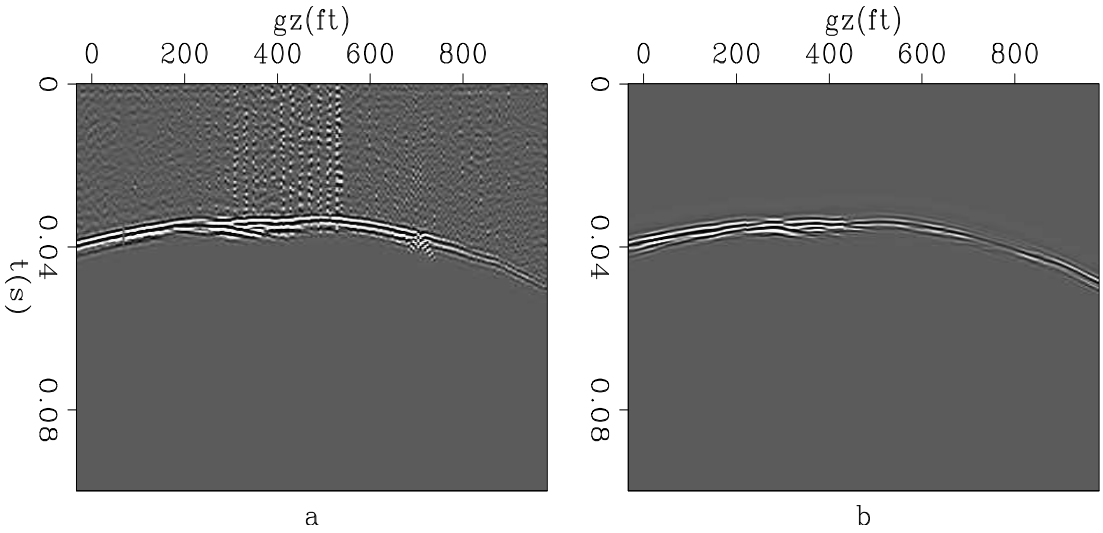

Figure 9: Same shot gather as before, comparsion of input first arrival and data modeled from the final inversion result. First arrival modeled from final result matches input kinematics very well. Left: Input first arrival; right: first arrival modeled from the final result. [**NR**]

CONCLUSIONS

A cross-well dataset was acquired to more accurately identify the boundary of an anomalous zone between the two wells. We applied early-arrival waveform inversion to the dataset. By trying to match recorded first arrivals, waveform inversion produced a much higher-resolution result than did traveltime tomography results. The boundary of the anomalous zone is more sharply defined. Details from the waveform inversion result is verified by the well-log data. Comparison of forward-modeled data with input data also suggests that wave-equation based methods predict data better than ray-based methods.

ACKNOWLEDGMENTS

We would like to thank Chevron for allowing us to publish the research results. We would also like to thank the Center for Computational Earth Sciences for providing the computation environment.

REFERENCES

Hampson, D. and B. Russell, 1984, First-break interpretation using generalized linear inversion: Journal of Canadian Society of Exploration Geophysicists, **20**, 40–54.

Harris, J. M., R. C. Nolen-Hoeksema, R. T. Langan, M. V. Schaack, S. K. Lazaratos, and J. W. Rector, 1995, High-resolution crosswell imaging of a west Texas carbonate reservoir: Part i-project summary and interpretation: Geophysics, **20**, 667–681.

Langan, R. T., A. A. Vassiliou, S. K. Lazaratos, T. L. Jensen, J. M. Harris, and J. W. Fairborn, 1997, Carbonate seismology: Chapter 17, Imaging of a Stratigraphically Complex Carbonate Reservoir with Crosswell Seismic Data.

Mora, P., 1987, Elastic wavefield inversion: Stanford Exploration Project Ph.D. Thesis.

Olson, K. B., 1984, A stable and flexible procedure for the inverse modelling of seismic first arrivals: Geophysical Prospecting, **37**, 455–465.

Pratt, R. G., C. Shin, and G. Hicks, 1998, Gauss-Newton and full Newton methods in frequency domain seismic waveform inversion: Geophysical Journal International, **133**, 341–362.

Shen, X., 2010, Near-surface velocity estimation by weighted early-arrival waveform inversion: SEG Expanded Abstracts, **29**, 1975–1979.

Tarantola, A., 1984, Inversion of seismic reflection data in the acoustic approximation: Geophysics, **49**, 1259–1266.

White, D. J., 1989, Two-dimensional seismic refraction tomography: Geophysical Journal International, **97**, 223–245.

Zelt, C. A. and P. J. Barton, 1998, 3D seismic refraction tomography: A comparison of two methods applied to data from the Faeroe Basin: Journal of Geophysical Research, **103**, 7187–7210.

Zhu, T. and J. M. Harris, 2011, Iterative joint inversion of P-wave and S-wave crosswell traveltime data: SEG Expanded Abstracts, **30**, 479–483.